



Natural Resources Conservation Service
National Soil Survey Center
Federal Building, Room 152
100 Centennial Mall North
Lincoln, NE 68508-3866

Phone: (402) 437-5499
FAX: (402) 437-5336

Subject: ENG -- Geophysical Assistance

Date: 30 January 2012

To: Denise C. Coleman
State Conservationist
USDA-NRCS,
Suite 340, One Credit Union Place
Harrisburg, PA 17110-2993

Purpose:

A large sinkhole and smaller dissolution features have developed close to one another in a cultivated field in Point Township, Northumberland County. The area affected by these features is approximately 9 m² and varies in depth from about 1.2 to 2.4 meters. Geophysical methods were used to identify the area and depth needing excavation for sinkhole treatment. In addition, geophysical methods were used to identify other potential sinkhole-prone areas within the field.

Participants:

Zachery Aukamp, Agricultural Engineer, USDA-NRCS, Bloomsburg, PA
Tim Craul, MLRA Project Leader, USDA-NRCS, University Park, PA
Jim Doolittle, Research Soil Scientist, USDA-NRCS-NSSC, Newtown Square, PA
Gary Gallup, Soil Conservation Technician, USDA-NRCS, Bloomsburg, PA
Mark Groshek, Engineering Technician (Civil), USDA-NRCS, Bloomsburg, PA
Donald Murray, Civil Engineer, USDA-NRCS, Bloomsburg, PA
Timothy Peters, Agricultural Engineer, USDA-NRCS, Bloomsburg, PA
Yuri Plowden, Resource Soil Scientist, USDA-NRCS, Bloomsburg, PA

Activities:

All field activities were completed during the period of 17 to 18 January 2012.

Summary:

1. Geophysical interpretations are considered preliminary estimates of site conditions. The results of geophysical investigations are interpretive and do not substitute for direct ground-truth observations (core sampling). The use of geophysical methods can reduce the number of cores, direct their placement, and supplement their interpretations. Interpretations contained in this report should be verified by ground-truth observations.
2. Both EMI and GPR provided some useful subsurface information. However, neither technique provided totally satisfactory results at this site. While GPR provided some, EMI provided little information concerning the depth or extensiveness of the sinkhole.
3. The suitability of EMI depends on such site-specific conditions as soil types, depth to bedrock, and size and composition of the dissolution features. Detection depends on the contrast in the measured physical property between the buried dissolution feature and the surrounding soil and

Helping People Help the Land

An Equal Opportunity Provider and Employer



bedrock. Detection also depends on local ground conditions, absence of interfering cultural features, and the sensitivity and observation depths of a particular meter. At this site, the moist, medium-textured soils lack sufficient contrast with the underlying bedrock and the size of subsurface dissolution features, if present, is believed to be too small to be clearly distinguished with the EM31 meter.

4. The presence of additional large dissolution features within the survey areas was not evident in the EC_a data. Three weakly expressed anomalous areas, which may be associated with dissolution features, were identified in Field 1.
5. The 200 MHz antenna provided a better balance of penetration depth and resolution than the 70 MHz antenna and was used to traverse the area surrounding the sinkhole. Unfortunately, the SIR-3000's GPS option failed after only two passes with the 200 MHz and only data from the north side of the sinkhole was properly georeferenced.
6. A GPR traverse located close to sinkhole revealed an area of subsidence consisting of high-amplitude subsurface reflections. The slumped, subsurface reflection pattern is estimated to be about 6 meter wide and consists of several interfaces identified by their dissimilar spatial patterns and polarity reversals of the reflected signal. A vertical conduit or cavity was also inferred by a clustering of high-amplitude, hyperbolic reflections beneath the lower, eastern portion of this subsurface reflection pattern. This feature appears to taper downward from the base of the previously discussed subsurface reflection pattern (at an estimated depth of about 2.9 m) to an estimated depth of about 4.2 m. This narrower feature is estimated to be about 1 m wide at its top.

It was the pleasure of Jim Doolittle and the National Soil Survey Center to provide this assistance to you and your staff.

/s/ Jonathan W. Hempel

JONATHAN W. HEMPEL
Director
National Soil Survey Center

cc: See attached list

cc:

Bob Dobos, Research Soil Scientist & Liaison for MO13, Soil Survey Research & Laboratory Staff,
USDA-NRCS-NSSC, Lincoln, NE
Jim Doolittle, Research Soil Scientist, USDA-NRCS-NSSC, Newtown Square, PA
Chuck Gordon, Acting Director of Soils Survey Division, USDA-NRCS, Washington, DC
Mark Groshek, Engineering Technician (Civil), USDA-NRCS, Bloomsburg, PA
Rob Knight, Acting State Soil Scientist, USDA-NRCS, Harrisburg, PA
Hosea Latshaw, State Conservation Engineer, USDA-NRCS, Harrisburg, PA
Yuri, Plowden, Resource Soil Scientist, USDA-NRCS, Bloomsburg, PA
Wes Tuttle, Soil Scientist (Geophysical), USDA-NRCS-NSSC, Wilkesboro, NC
Larry West, National Leader, Soil Survey Research & Laboratory, USDA-NRCS-NSSC, Lincoln, NE

Technical Report on Geophysical Investigations conducted in Point Township, Northumberland County, Pennsylvania on 17 to 18 January 2012.

James A. Doolittle

Background:

After heavy rains in mid-September 2011, a large sinkhole and two smaller dissolution features developed close to one another in a cultivated field located in Point Township, Northumberland County. The field had been planted to corn. During harvesting, a combine fell into the sinkhole and needed to be pulled out. The area affected by the sinkhole and dissolution features is approximately 9 m² and varies in depth from 1.2 to 2.4 meters.

The Pennsylvania State Office requested assistance from the National Soil Survey Center to survey the area surrounding the sinkhole and dissolution features with electromagnetic induction (EMI) and ground-penetrating radar (GPR) prior to the application of *Sinkhole and Sinkhole Area Treatment* (Practice Code 527).

Use of Geophysical Methods in Areas of Karst:

Risks associated with groundwater contamination and the collapse or subsidence of the ground surface are inherent in areas of karst. Traditionally, remote sensing and borehole observations have been used to acquire information on the distribution of major dissolution features. Aerial photographs permit the examination of large areas and the identification of some sinkholes and fracture patterns. However, many structural and dissolution features lack surface expression and are not detectable on aerial photographs. Borehole surveys provide detailed subsurface information. However, these surveys are relatively expensive and data are restricted to the points of observation. In areas of karst, subsurface properties can be highly variable over short distances and extrapolations made from a limited number of widely spaced borehole logs can be flawed (Collins et al., 1990 and 1994). Alternative methods are needed to complement traditional methods and to improve site assessments.

Geophysical methods can provide ancillary subsurface information for hazard estimation and groundwater vulnerability assessments in areas of karst (Chalikakis et al., 2011). Two geophysical methods frequently used in areas of karst are EMI and GPR. Electromagnetic induction has been used to identify and map sinkholes, cavities, fractures, bedrock surfaces, and preferential infiltration pathway (Valois et al., 2011; Jardani et al. 2007; Wedekind et al., 2005; Ahmed and Carpenter, 2003; Carpenter, and Ahmed, 2002; Rumbens, 1990; Pazuniak, 1989; Robinson-Poteet, 1989; Canace and Dalton, 1984). Ground-penetrating radar has been used to characterize bedrock surfaces and bedding planes, detect dissolution features, and delineate fractured and *karstified* zones in bedrock (Estrada-Medina et al., 2010; Pueyo-Anchuela et al., 2009; Al-fares et al., 2002; Batayneh et al., 2002; Mellett and Maccarillo, 1995; Wilson, 1995; Collins et al., 1994 and 1990; Puckett et al., 1990; Barr, 1993; Hearn, 1987; Carter et al., 1986; Ballard, 1983). However, these methods do not work equally well in all areas of karst. In addition, the amount of practical information derived from surveys has varied. The most appropriate methodology often depends on such site-specific conditions as soil types, depth to bedrock, and size and composition of the structural or dissolution features.

Electromagnetic induction uses electromagnetic energy to measure the apparent conductivity (EC_a) of earthen materials. Apparent conductivity is a depth weighted, average conductivity measurement for a column of earthen materials (Greenhouse and Slaine, 1983). Variations in EC_a are produced by changes in the electrical conductivity of earthen materials. The electrical conductivity of soils is influenced by water content, type and concentration of ions in solution, temperature and phase of the soil water, and

amount and type of clays in the soil matrix (McNeill, 1980b). The EC_a of soils will increase with increasing soluble salts, water, and/or clay contents (Kachanoski et al., 1988; Rhoades et al., 1976). Electromagnetic induction measures vertical and lateral variations in EC_a . Values of EC_a are seldom diagnostic in themselves, but variations in measurements can be used to infer changes in soils and soil properties. Interpretations are based on the identification of spatial patterns within data sets.

Ground-penetrating radar (GPR) is an impulse radar system designed for shallow (0 to 30 m) subsurface investigations. This geophysical tool has the capacity to produce continuous, highly-detailed, cross-sectional profiles of the subsurface in a relatively fast manner. Ground-penetrating radar provides higher resolution, but is more depth restricted than EMI. The exploration depth of GPR is determined by antenna frequency and the electrical conductivity of the earthen materials being profiled (Daniels, 2003 and 2004). In general, the depth of exploration will increase with decreasing frequency. For a given antenna frequency, the depth of exploration is dependent on signal attenuation. Soils having high electrical conductivity rapidly attenuate radar energy, restrict penetration depths, and severely limit the effectiveness of GPR.

Equipment:

The EM31 meter manufactured by Geonics Limited (Mississauga, Ontario) was used in this study.¹ McNeill (1980a) has described the principles of operation for the EM31 meter. The EM31 meter has a 3.66-m intercoil spacing and operates at a frequency of 9,810 Hz. Lateral resolution is approximately equal to the intercoil spacing. The EM31 meter provides effective penetration depths of about 3.0 and 6.0 meters in the horizontal and vertical dipole orientations, respectively (McNeill, 1980a). The EM31 meter is portable and needs only one person to operate. No ground contact is required with this meter. The meter provides a depth-weight measure of the apparent conductivity (EC_a) of the underlying earthen materials. Values of EC_a are expressed in milliSiemens per meter (mS/m).

The Geonics DAS70 Data Acquisition System was used with the EM31 meter to record and store both EC_a and GPS data.¹ The acquisition system consists of the EM31 meter, an Allegro CX field computer (Juniper Systems, Logan, Utah), and a Trimble AgGPS 114 L-band DGPS (differential GPS) (Trimble, Sunnyvale, CA).¹ With the acquisition system, the EM31 meter is keypad operated and measurements can either be automatically or manually triggered. The RTM31 program (Geomar Software, Inc., Mississauga, Ontario) was used with the EM31 meter to display and record both GPS and EC_a data on the Allegro CX field computer.¹

To help summarize the results of the EMI surveys, the SURFER for Windows (version 10) program, developed by Golden Software, Inc., was used to construct two- and three-dimensional simulations.¹ Grids were created using kriging methods with an octant search.

The radar unit is the TerraSIRch Subsurface Interface Radar (SIR) System-3000 (here after referred to as the SIR-3000), manufactured by Geophysical Survey Systems, Inc. (GSSI; Salem, NH).¹ The SIR-3000 consists of a digital control unit (DC-3000) with keypad, SVGA video screen, and connector panel. A 10.8-volt lithium-ion rechargeable battery powers the system. The SIR-3000 weighs about 4.1 kg (9 lbs) and is backpack portable. With an antenna, the SIR-3000 requires two people to operate. Jol (2009) and Daniels (2004) discuss the use and operation of GPR. The 70 and 200 MHz antennas were used in this study.

The RADAN for Windows (version 6.6) software program (GSSI) was used to process the radar records.¹ Processing included: header editing, setting the initial pulse to time zero, color table and transformation

¹ Trade names are used to provide specific information. Their mention does not constitute endorsement by USDA-NRCS.

selection, signal stacking, migration, horizontal high pass filtration, and range gain adjustments (refer to Jol (2009) and Daniels (2004) for discussions of these techniques).

Recent technical developments allow the integration of GPR and GPS data. The SIR-3000 system provides a setup for the use of a GPS receiver with a serial data recorder (SDR). With this setup, each radar scan is georeferenced (position/time matched). Following data collection, a subprogram within RADAN is used to proportionally adjust the position of each radar scan according to the time stamp of the two nearest positions recorded with the GPS receiver. A Trimble AgGPS114 L-band DGPS antenna (Trimble, Sunnyvale, CA) was used to collect position data.¹ Position data were recorded at a rate of one measurement per second. The scanning rate of the GPR was set at 42 scan/sec.

Calibration of GPR:

Ground-penetrating radar is a time scaled system. The system measures the time that it takes electromagnetic energy to travel from an antenna to an interface (e.g., soil horizon, stratigraphic layer, bedrock) and back. To convert the travel time into a depth scale, either the velocity of pulse propagation or the depth to a reflector must be known. The relationships among depth (D), two-way pulse travel time (T), and velocity of propagation (v) are described in equation [1] (after Daniels, 2004):

$$v = 2D/T \quad [1]$$

The velocity of propagation is principally affected by the relative dielectric permittivity (E_r) of the profiled material(s) according to equation [2] (after Daniels, 2004):

$$E_r = (C/v)^2 \quad [2]$$

Where C is the velocity of propagation in a vacuum (0.298 m/ns). In soils, the amount and physical state (temperature dependent) of water have the greatest effect on the E_r and v . Dielectric permittivity ranges from 1 for air, to 78 to 88 for water (Cassidy, 2009).

Based on the measured depth and the two-way pulse travel time to known subsurface reflectors (buried metal plate at 50 cm, and bedrock at 117 cm), the velocity of propagation and the relative dielectric permittivity through the upper part of the soil profile were estimated using equations [1] and [2]. The estimated E_r and v were 6.4 and 0.1178 m/ns, respectively. The upper 10 cm of the soil was frozen at the time of this investigation.

Survey Area:

The sinkholes (latitude 40.9143 N latitude, 76.8294 W longitude) are located in a cultivated field in Point Township, Northumberland County (Figure 1). The sinkholes developed in an area that is mapped as Washington silt loam, wet substratum, 3 to 8 % slopes (map unit WaB). The very deep, well drained Washington soils formed in old glacial drift (pre-Wisconsin Age) or colluvium derived mainly from limestone. Other soil delineations mapped within the survey area include: Allenwood and Washington soils, 8 to 15 % slopes (AoC); Elliber cherty silt loam, 8 to 15 % slopes (EsC); and Kreamer cherty silt loam, 3 to 8 % slopes (KMB). The taxonomic classifications of these soils are listed in Table 1. An area mapped as Pits (Pa) borders the northern boundary of Field 1 (field that contains sinkhole).

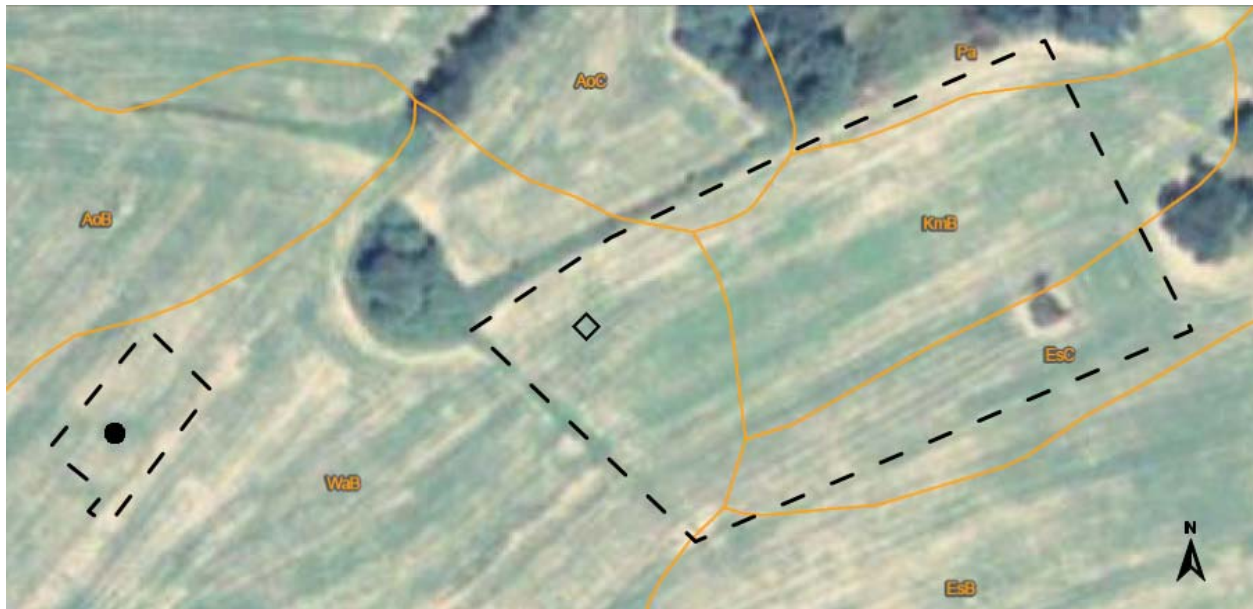


Figure 1. This soil map from the Web Soil Survey shows the approximate locations of the two survey areas, the sinkhole (◇), and the ponded area (●).

Table 1. Taxonomic Classification of the soils recognized within the survey areas.

Soil Series	Taxonomic Classification
Allenwood	Fine-loamy, mixed, semiactive, mesic Typic Hapludults
Elliber	Loamy-skeletal, mixed, semiactive, mesic Typic Hapludults
Kreamer	Fine, illitic, mesic Aquic Hapludults
Washington	Fine-loamy, mixed, semiactive, mesic Ultic Hapludalfs.

Field Procedures:

The EM31 meter was operated in the continuous mode with measurements recorded at a 0.5 sec interval using the DAS70 Data Acquisition System. The EM31 meter was held at hip height with its long axis orientated orthogonal (broadside) to the direction of travel. Surveys were carried out with the EM31 meter operated in the vertical dipole orientation. Walking at a fairly uniform pace in a back and forth manner across each field completed the EMI survey.

Radar traverses were completed with both the 70 and 200 MHz antenna near the sinkholes in Field 1. Traverses were conducted between rows of corn stubble located both up-slope and down-slope to the sinkhole. The GPS option malfunctioned and was unavailable for all but two radar traverses.

Results:

EMI:

Apparent conductivity was low and invariable across the two fields. Basic statistics for the two fields were nearly identical. In Field 1, EC_a averaged only 8.3 mS/m and ranged from about 4.0 to 36.0 mS/m. One-half the EC_a measurements were between about 7.1 and 9.2 mS/m. Anomalously high EC_a data were recorded beneath power lines that stretched from north to south across the eastern portion of Field 1. In Field 2, EC_a averaged only 8.7 mS/m and ranged from 7.2 to 10.8 mS/m. One-half the EC_a measurements were between about 8.0 and 9.2 mS/m.

Table 2. Basic Statistics for the EMI surveys that were completed within Fields 1 and 2.

	Field 1	Field 2
Number	8356	1083
Minimum	4.00	7.20
25%-tile	7.13	8.00
75%-tile	9.20	9.20
Maximum	35.90	10.80
Mean	8.29	8.67
Std. Dev.	2.61	0.82

Figure 2 contains plots of the EC_a data collected with the EM31 meter across Field 1. Soil boundary lines have been digitized from Web Soil Survey data². In Figure 2, a majority of the spatial patterns appear to trend in a southwest to northeast direction. As this orientation conforms to the general strike of the bedrock, perceived differences in EC_a are associated largely with differences in the lithology and/or depth to bedrock. Because of higher clay and moisture contents, the overlying soil mantle is presumed to have a higher EC_a than the underlying limestone bedrock. As a consequence, thicker soil columns with deeper depths to bedrock are associated with higher EC_a. Conversely, thinner soil columns having shallower depths to more electrically resistive bedrock are associated with lower EC_a.

Electromagnetic induction is susceptible to interference from cultural features. The anomalous, linear pattern in the eastern portion of Field 1 (Figure 2) is caused by electrical interferences from overlying transmission lines.

The area with the sinkhole and dissolution features has been identified with a spot symbol in Figure 2. In areas of karst, the appropriateness of EMI often depends on the soil types, depth to bedrock, and size and composition of the structural or dissolution features. Detection depends on the contrast in the measured physical property (EC_a) between the dissolution feature and the surrounding soil and bedrock. Large air-filled cavities or plugged dissolution features are more detectable than small voids or cavities filled with rock fragments. There is a tendency for EMI to smooth, suppress, or even omit the expression of subsurface features that have widths smaller than the intercoil spacing of the meter. In addition, detection depends on local ground conditions, absence of interfering cultural features, and the sensitivity and observation depths of a particular meter. At this site, the moist, medium-textured soils appear to lack sufficient contrast with the underlying bedrock, and the size of subsurface dissolution features, if present, is believed to be too small to be clearly distinguished with the EM31 meter.

The sinkhole and dissolution features are located in a slight topographic swale that extends towards the northeast and into an adjoining field. In Figure 2, this swale is expressed as a zone of slightly higher EC_a (9 to 10 mS/m). The higher EC_a within this swale is attributed to higher moisture and possibly clay contents of the soils. In Figure 2, the area of the sinkhole appears to interrupt this pattern of slightly higher EC_a that is attributed to the swale. Though very weakly expressed, three additional anomalies have been identified in Figure 2 (see *A*, *B*, and *C*). Faint, nearly circular spatial patterns of slightly lower EC_a are used to identify anomalies *A* and *B*. Anomaly *A* occurs in a depressional area located to the east of the sinkhole. As this area is presumably wetter and has been infilled with finer-textured slope washed materials, the slightly lower measured EC_a is anomalous and may identify an air-filled void beneath this depression. Anomaly *C* is identified by its higher EC_a. This feature could represent a clay-filled paleo-

² Soil Survey Staff, Natural Resources Conservation Service, United States Department of Agriculture. Web Soil Survey. Available online at <http://websoilsurvey.nrcs.usda.gov/> accessed [01/20/2012].

sink or a unit of slightly finer-textured soil materials.

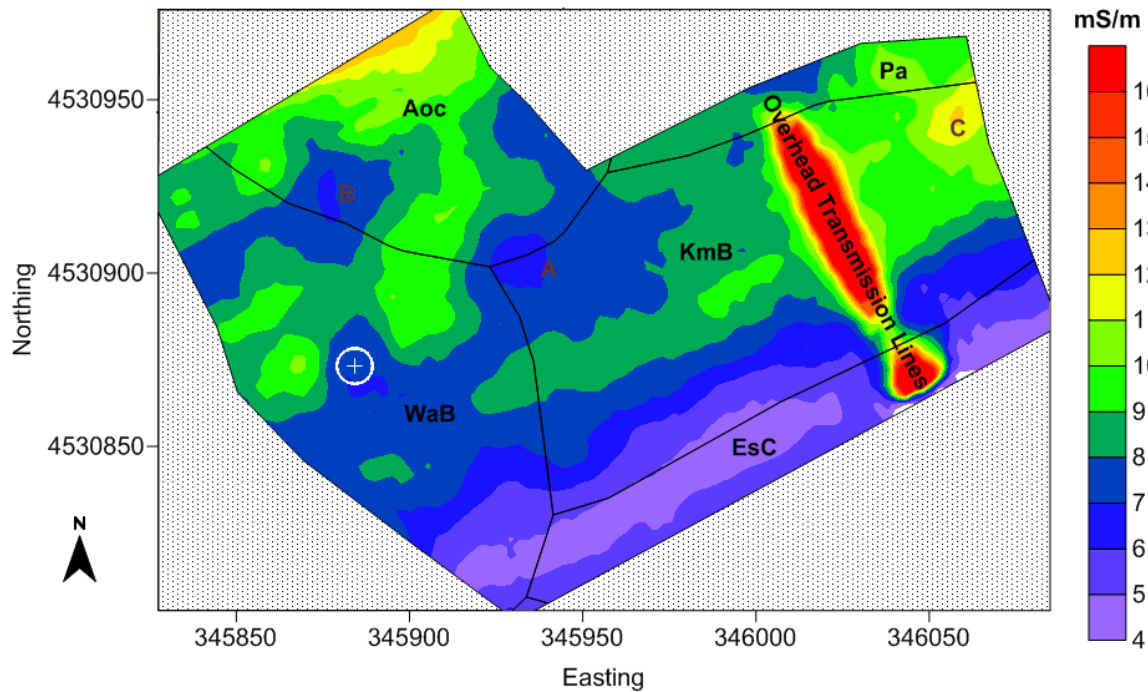


Figure 2. These spatial EC_a patterns were obtained in Field 1 with an EM31 meter operated in the VDO. The approximate location of the sinkholes is identified by the spot symbol. Soil lines are from the Web Soil Survey.

Figure 3 is a three-dimensional simulation of the area surveyed in Field 1. Elevation data used to construct this simulation were derived from GPS measurements. This simulation highlights the relative location of the sinkhole within the landscape. Evident in this plot is the interruption of a zone of slightly higher EC_a , which is attributed to wetter soil conditions in a minor topographic swale, by the dissolution features.

The landowner was interested in having an EMI survey conducted across a small, ponded depression in an adjoining field. Figure 4 shows the results of this survey. In Figure 4, the approximate location of the ponded area is identified by a spot symbol. Apparent conductivity was exceedingly low and invariable across this site (see Table 2). Because of this invariability, an isoline interval of 0.5 mS/m has been used in this plot to highlight the weakly-expressed spatial EC_a patterns. As instrument and calibration errors can account for errors of 1 to 2 mS/m, the spatial patterns shown in this simulation should be viewed with modest reservations. In Figure 4, no indication of the ponded area is evident. However, a noticeable zone of higher EC_a is evident to the immediate northeast of this depression. As this pattern occurs on a higher-lying area, the increase EC_a is principally attributed to an increase in clay content or depth to bedrock. The proximity of this pattern to the ponded depression may warrant additional coring to confirm the factors or features involved.

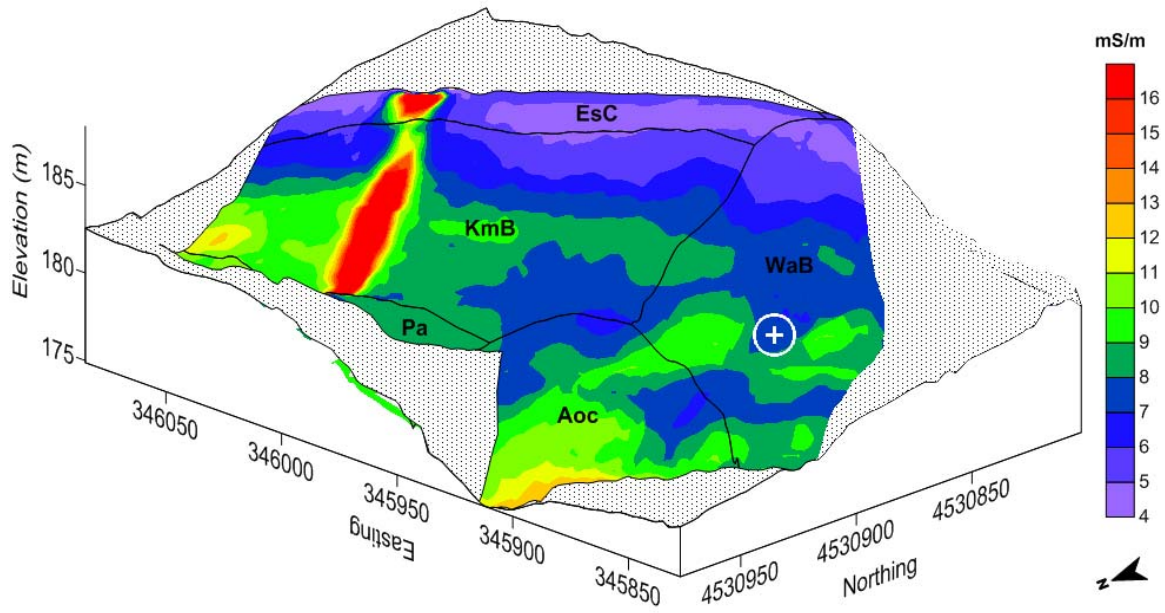


Figure 3. Elevation data used to construct this three-dimensional (3D) simulation of the EC_a data collected in Field 1 were derived from GPS measurements. The approximate location of the sinkholes is identified by the spot symbol. Soil lines are from the Web Soil Survey.

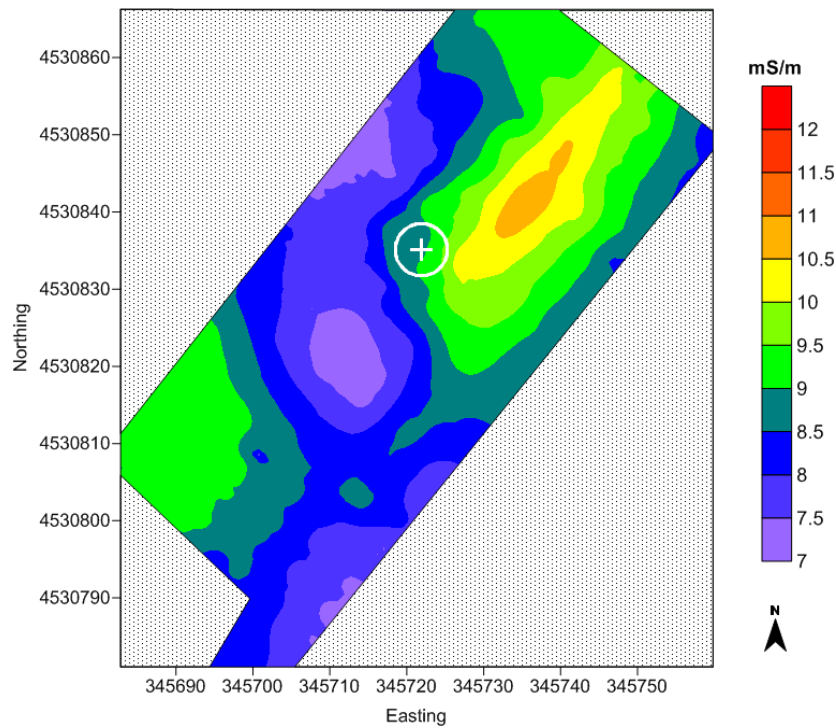


Figure 4. These spatial EC_a patterns were obtained in Field 2 with an EM31 meter operated in the VDO. The approximate location of the ponded area is identified by the spot symbol. Soil lines are from the Web Soil Survey.

GPR:

The 200 MHz antenna provided a better balance of penetration depth and resolution than the 70 MHz antenna and was used to traverse the area surrounding the sinkhole. Unfortunately, the SIR-3000's GPS option failed after only two passes with the 200 MHz and only the north side of the sinkhole was properly surveyed. The locations of these two traverses are shown in Figure 5. An additional traverse was conducted on the south side of the sinkhole area. However, this traverse could not be accurately georeferenced.

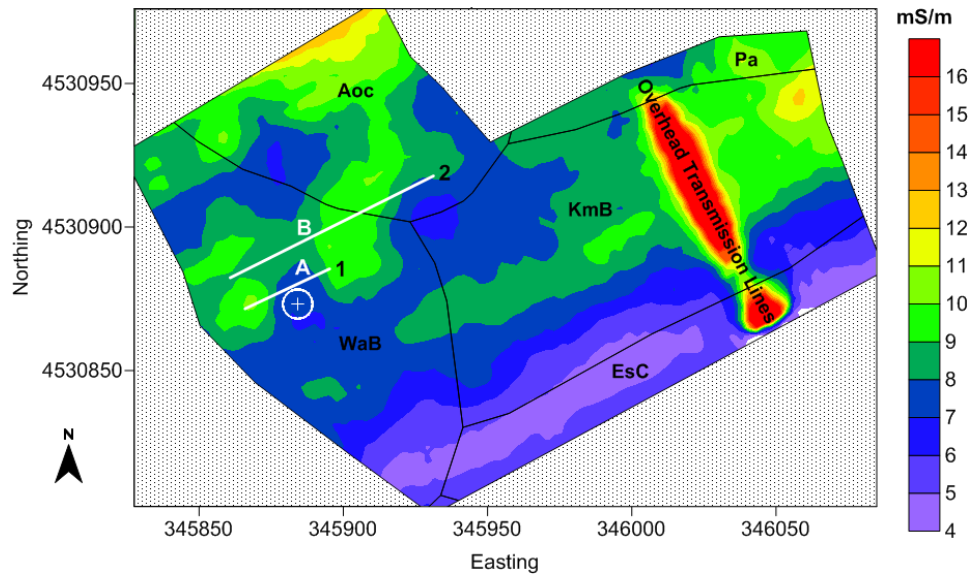


Figure 5. The locations of two GPR traverse lines are shown on this plot of spatial EC_a patterns in Field 1. The approximate location of the sinkholes is identified by the spot symbol. Soil lines are from the Web Soil Survey.

Figure 6 and 7 are three-dimensional (3D) pseudo images of the radar record collected along Lines 1 and 2, respectively. In these pseudo images, all units of measurements are expressed in meters. The UTM geographic coordinate system is used in these images. In each image, a green-colored segmented line has been used to identify the interpreted soil/bedrock interface.

The GPR traverse shown in Figure 6 was conducted closest to sinkhole (see Figure 5 for location). This GPR image reveals an area of subsidence with anomalous, high-amplitude subsurface reflection patterns (see “A” in Figure 6). Slumped, near surface soil horizons are often caused by water infiltration and associated with lower-density soil materials and dissolution activity in the deeper limestone formation. This subsurface reflection pattern is estimated to be about 6 meter wide and consists of several interfaces identified by their dissimilar spatial patterns and reversal in the polarity of the reflected signal. A soil core, extracted near this spatial pattern's lowest point, met with refusal at a depth of 117 cm. This depth was taken as the depth to the underlying bedrock. In Figure 6, a vertical conduit or cavity can also be inferred by the clustering of high-amplitude, hyperbolic reflections beneath the lower, eastern portion (right-hand) of this subsurface reflection pattern. This feature appears to taper downward from the base of the previously noted subsurface anomaly (at an estimated depth of about 2.9 m) to an estimated depth of about 4.2 m. This feature is estimated to be about 1 m wide at its top.

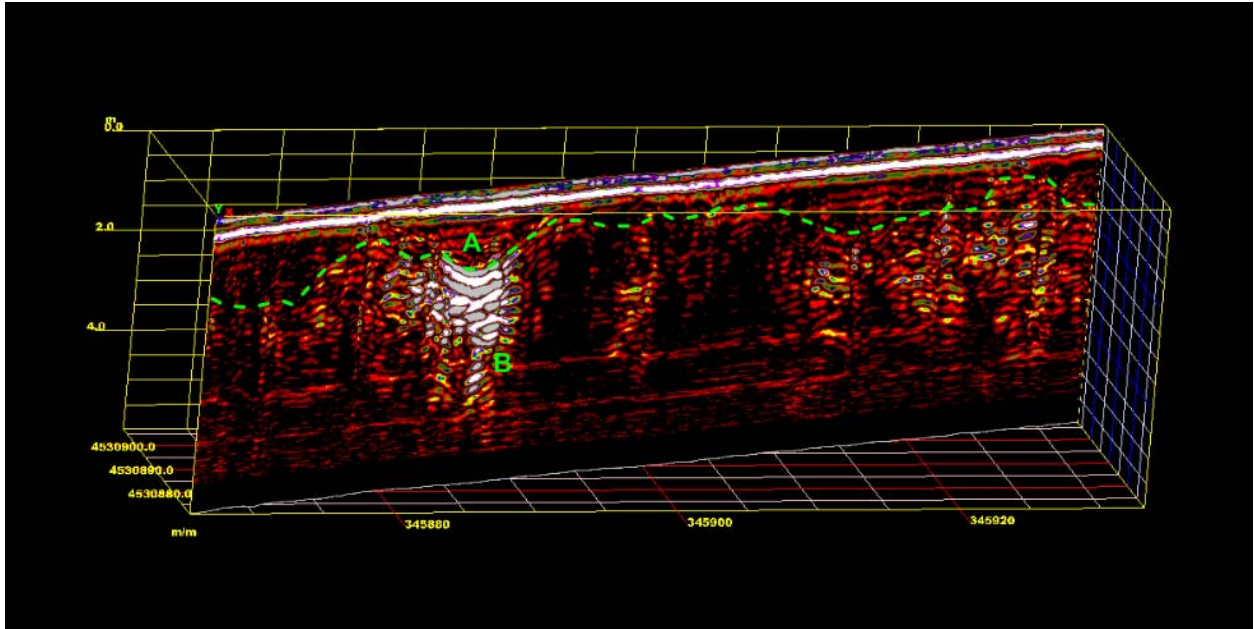


Figure 6. In this 3D image of the radar record collected along line 1, the interpreted depth to bedrock is identified by a segmented green-colored line. An anomalous feature worthy of further study is shown at A.

Figure 7 is a three-dimensional (3D) pseudo image of the radar record collected along Line 2. This GPR image reveals no anomaly similar to the one identified in Figure 5 for Line 1. A radar traverse was also conducted to the south side of the sink, but lacking GPS, the line was poorly associated with the location of the sinkhole. However, on the radar record from the south side of the sinkhole (not shown), the imagery is similar to that on Line 2 (with no anomaly such as shown at “A” along Line 1).

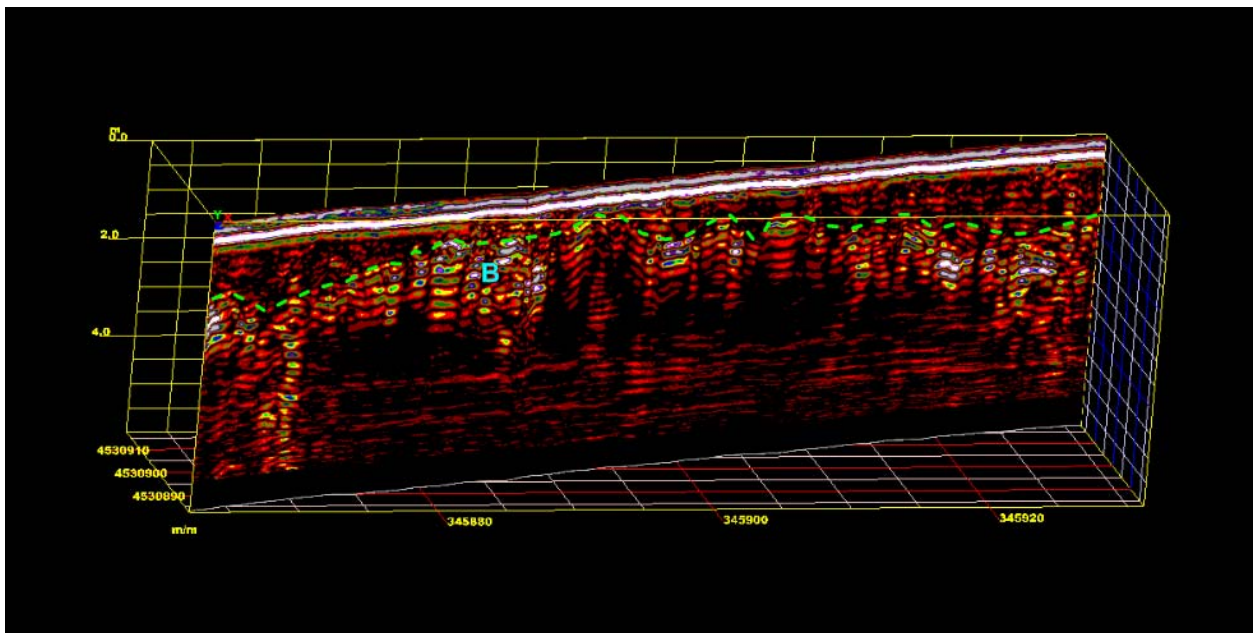


Figure 7. In this 3D image of the radar record collected along line 2, the interpreted depth to bedrock is identified by a segmented green-colored line.

References:

- Ahmed, S., and P. J. Carpenter, 2003. Geophysical response of filled sinkholes, soil pipes and associated bedrock fractures in thinly mantled karst, east-central Illinois. *Environmental Geology* 4: 705-716.
- Al-fares, W., M. Bakalowicz, R. Guérin, M. Dukhan, 2002. Analysis of karst aquifer structure of the Lamalou area (Hérault, France) with ground-penetrating radar. *Journal of Applied Geophysics* 51: 97-106.
- Ballard, R. F. Jr., 1983. Cavity detection and delineation research. Report No. 5: Electromagnetic (radar) techniques applied to cavity detection. US Army Corps of Engineers, Waterways Experiment Station, Vicksburg, Mississippi. Tech. Report GL-83-1. pp. 90.
- Barr, G. L., 1993. Application of ground-penetrating radar methods in determining hydrogeologic conditions in a karst area, west-central Florida. USGS Water Resources Investigation Report 92-4141. pp. 26.
- Batayneh, A. T., A. A. Abueladas, K. A. Moumani, 2002. Use of ground-penetrating radar for assessment of potential sinkhole conditions: an example from Ghor al Haditha area, Jordan. *Environmental Geology* 41: 977-983.
- Canace, R. and R. Dalton, 1984. A geological survey's cooperative approach to analyzing and remedying a sinkhole related disaster in an urban environment. pp. 342-348. *In: Proceedings of the First Multidisciplinary Conference on Sinkholes*. Orlando, Florida. October 15 to 17, 1984.
- Carpenter, P. J., and S. Ahmed, 2002. Detecting preferential infiltration pathways in soils using geophysics. *Leading Edge* May 2002: 471-473.
- Carter, T. G., M. L. J. Mahner, A. P. Annan, and J. A. Richard, 1986. Specialized investigation techniques for defining karstic cavities. pp. 345-367. *In: Proceedings of the Environmental Problems in Karst Terranes and their Solutions Conference*. National Water Well Association. Dublin, Ohio.
- Cassidy, N.J. 2009. Electrical and magnetic properties of rocks, soils, and fluids. In *Ground Penetrating Radar: Theory and Applications*, ed. H. M. Jol, 41-72 pp. Elsevier Science, Amsterdam, The Netherlands.
- Chalikakis, K., V. Plagnes, R. Guerin, R. Valois, and F. P. Bosch, 2011. Contribution of geophysical methods to karst-system exploration: an overview. *Hydrogeology Journal* 19: 1169-1180.
- Collins M. E., W. E. Puckett, G. W. Schellentrager, and N. A. Yust, 1990. Using GPR for micro-analyses of soils and karst features on the Chiefland Limestone Plain in Florida. *Geoderma* 47:159-170.
- Collins, M. E., M. Crum, and P. Hanninen, 1994. Using ground-penetrating radar to investigate subsurface karst landscape in north-central Florida. *Geoderma* 61:1-15.
- Daniels, J. J., B. Allred, M. Collins, and J. Doolittle. 2003. Geophysics in Soil Science. 1-5 pp. In: Lal, R. (ed.) *Encyclopedia of Soil Science*. Marcel Dekker, Inc., New York, New York.
- Daniel D., 2004. *Ground Penetrating Radar, 2nd Edition*. The Institute of Electrical Engineers, London, United Kingdom.
- Estrada-Medina, H., W. Tuttle, R. C. Graham, M. F. Allen, and J. J. Jiménez-Osornio, 2010.

- Identification of underground karst features using ground-penetrating radar in Northern Yucatán, México. *Vadose Zone Journal* 9: 653-661.
- Greenhouse, J. P., and D. D. Slaine. 1983. The use of reconnaissance electromagnetic methods to map contaminant migration. *Ground Water Monitoring Review* 3(2): 47-59.
- Hearns, D. J., 1987. The application of ground-penetrating radar to geologic investigations in karst terrains. M. Sc. Thesis. University of Florida, Gainesville, Fl. pp. 107.
- Jardani, A., A. Revil, E. Santos, C. Fauchard, and J. P. Dupont, 2007. Detection of preferential infiltration pathways in sinkholes using joint inversion of self-potential and EM-34 conductivity data. *Geophysical Prospecting*. 55 (5): 749-760
- Kachanoski, R. G., E. G. Gregorich, and I. J. Van Wesenbeeck. 1988. Estimating spatial variations of soil water content using noncontacting electromagnetic inductive methods. *Canadian Journal of Soil Science* 68:715-722.
- McNeill, J. D. 1980a. Electromagnetic terrain conductivity measurement at low induction numbers. Technical Note TN-6. Geonics Limited, Mississauga, Ontario. p. 15.
- McNeill, J. D. 1980b. Electrical Conductivity of soils and rocks. Technical Note TN-5. Geonics Ltd., Mississauga, Ontario. p. 22.
- Mellett, J. S. and B. J. Maccarillo, 1995. A model for sinkhole formation on interstate and limited access highways, with suggestions on remediation. p. 335-339. In: Beck, B. F. (ed.) *Karst GeoHazards*. A. A. Balkema, Rotterdam.
- Pazuniak, B. L., 1989. Subsurface investigation response to sinkhole activity at an eastern Pennsylvania site. p. 263-269. In: Proceedings of the 3rd Multidisciplinary Conference on Sinkholes. St. Petersburg Beach, Florida. 2 to 4 October 1989.
- Puckett, W. E., M. E. Collins, and G. W. Schellentrager, 1990. Design of soil map units on a karst area in west central Florida. *Soil Science Society of America Journal* 54:1068-1073.
- Pueyo-Anchuela, Ó. A. Pocoví, M. A. Soriano, and A. M. Casa-Sainz, 2009. Characterization of karst hazards from the perspective of doline triangle using GPR – Examples from Central Ebro Basin (Spain). *Engineering Geology* 108: 225-236.
- Rhoades, J. D., P. A. Raats, and R. J. Prather. 1976. Effects of liquid-phase electrical conductivity, water content, and surface conductivity on bulk soil electrical conductivity. *Soil Science Society of America Journal* 40:651-655.
- Robinson-Poteet, D., 1989. Using terrain conductivity to detect subsurface voids and caves in a limestone formation. p. 271-279. In: Proceedings of the 3rd Multidisciplinary Conference on Sinkholes. St. Petersburg Beach, Florida. 2 to 4 October 1989.
- Rumbens, A. J., 1990. Detection of cavities in karstic terrain: road subsidence - Snowy Mountains Highway near Yarrangobilly, State of New South Wales - Australia. *Exploration Geophysics* 21:121-24.

Valois, R., C. Camerlynck, A. Dhemaied, R. Guerin, G. Hovhannissian, V. Plagnes, F. Rejiba, and H. Robain, 2011. Assessment of doline geometry using geophysics on the Quercy Plateau karst (South France). *Earth Surface Processes and Landforms* 36: 1183-1192.

Wedekind, J. E., M. A. Osten, E. Kitt, and B. Herridge, 2005. Combining surface and downhole geophysical methods to identify karst conditions in North-central Iowa. *Geotechnical Special Publication* 144: 616-625.

Wilson, W. L., 1995. Sinkhole and buried sinkhole densities and new sinkhole frequencies in karsts of northwest Peninsular Florida. p. 79-91. In: Beck, B. F. (ed.) *Karst GeoHazards*. A. A. Balkema, Rotterdam.